

# Mechanical design, modeling, and identification for a novel antagonistic variable stiffness dexterous finger

Handong HU, Yiwei LIU (✉), Zongwu XIE, Jianfeng YAO, Hong LIU

*State Key Laboratory of Robotics and System, Harbin Institute of Technology, Harbin 150001, China*

✉ Corresponding author. E-mail: lyw\_hit@163.com (Yiwei LIU)

© The Author(s) 2022. This article is published with open access at link.springer.com and journal.hep.com.cn

**ABSTRACT** This study traces the development of dexterous hand research and proposes a novel antagonistic variable stiffness dexterous finger mechanism to improve the safety of dexterous hand in unpredictable environments, such as unstructured or man-made operational errors through comprehensive consideration of cost, accuracy, manufacturing, and application. Based on the concept of mechanical passive compliance, which is widely implemented in robots for interactions, a finger is dedicated to improving mechanical robustness. The finger mechanism not only achieves passive compliance against physical impacts, but also implements the variable stiffness actuator principle in a compact finger without adding supererogatory actuators. It achieves finger stiffness adjustability according to the biologically inspired stiffness variation principle of discarding some mobilities to adjust stiffness. The mechanical design of the finger and its stiffness adjusting methods are elaborated. The stiffness characteristics of the finger joint and the actuation unit are analyzed. Experimental results of the finger joint stiffness identification and finger impact tests under different finger stiffness presets are provided to verify the validity of the model. Fingers have been experimentally proven to be robust against physical impacts. Moreover, the experimental part verifies that fingers have good power, grasping, and manipulation performance.

**KEYWORDS** multifingered hand, mechanism design, robot safety, variable stiffness actuator

## 1 Introduction

Multifingered robotic hands have been used for grasping and manipulating tools in the early stages of robotic research to achieve precise manipulation of targets through finger movements [1], such as Stanford/JPL hand [2], Utah/MIT hand [3], NASA hand [4], DLR hands [5], and DLR-HIT hands [6]. However, the design of these dexterous hands is mainly aimed at grasping or operating objects in static or quasi-static state. It focuses on achieving bionic movement functions on mechanical devices. In fact, physical collisions are unavoidable when multifingered hands are exposed to unstructured environments, and the energy generated by impacts and vibrations can damage the hardware system of multifingered hands. Although compliance control can submit a multifingered hand to disturbances, it cannot withstand high-frequency external impacts due to delays associated with sensing, control, and communication [7,8]. Hence, the movements

of the hand require rigorous planning and operation on account of the fragile hardware of the fingers, thereby hindering the application of many manipulation strategies, such as grasping in environments where obstacles move quickly and interacting with humans or other robots. Human hands have certain impact resistance in the interaction process because of flexibility of tendons, joints, and muscles; they can repair injury caused by external impact energy because of the self-repairing ability of bio-tissues. As proposed in Refs. [9,10], the hardware system of multifingered hand is protected by absorbing impact energy through elastic materials, such as joints or fingers made of elastic materials, to achieve mechanical robustness. Although this scheme achieves passive compliance, it cannot satisfy high precision or strength manipulation requirements. A method of reducing system bandwidth by connecting an elastic element in series between link side and actuator is proposed to passively comply with the mechanical system and achieve safety and accuracy. In this method, the environmental impact energy from the link side is stored

by the elastic element and released slowly to protect the actuator and other components from damage, thereby achieving high mechanical robustness. Nevertheless, the actuators proposed in Refs. [11–14] are extremely large to be integrated into a compact robotic hand. Hence, Grebenstein et al. [15] proposed a compact, lightweight, tendon-driven mechanism based variable stiffness actuator (VSA) for robot hands and integrated it in the DLR hand arm system; as a result, the hand can withstand the impact of high speed. However, the mechanical system is complex and costly to manufacture and maintain. Ishikawa team [16] proposed a compact-size actuator called “MagLinkage” that applies magnetic coupler instead of rigid coupler in joint drive system and a three-fingered hand. The magnetic coupling of the MagLinkage is destructible without any structural damage under overload to protect the hand from damage. This hand can only grasp small objects due to the limited force capacity of the magnetic couplers. Based on the analysis of the properties (fingertip force, weight, accuracy, fabrication, and cost) of prevalent dexterous hands and the principle of passive compliance of mechanical system illustrated in Table 1 [17–26], this study proposes an antagonistic variable stiffness dexterous finger (AVS-finger) mechanism. Compared with the prevalent dexterous hand, the main goal is to use universal gears, motors, and more reliable mechanisms to achieve robustness of the dexterous hand against physical impacts. Therefore, the AVS-finger based on gear transmission tends to be more reliable and easier to manufacture and maintain than cable-driven dexterous hands. In addition, the finger has

the following characteristics: Adjust its mechanical stiffness according to different task requirements and enhance the dynamic performance of finger movement by storing energy.

This paper is organized as follows. In Section 2, the implementation of the VSA principle in the finger mechanism is elaborated. Section 3 carries out statics, mechanical stiffness, and energy modeling and derives the finger stiffness adjusting strategies. In Section 4, experiments are conducted to validate the manipulating, grasping, force, and robustness performance of the finger, identify the finger joint stiffness characteristics, and illustrate the results of the finger stiffness variation operation. Finally, conclusions with future work are summarized in Section 5.

## 2 Mechanical design of the finger based on VSA principle

Dexterous hands require not only anthropopathic grasping and manipulation characteristics, but also compliance to unpredictable physical impacts to guarantee their safety. The anti-impact ability of its finger, as the direct transmitter of movements and forces between the dexterous hand and the object, is very important to improve the overall mechanical robustness of the hand. VSA principle has been widely implemented in various interactive robots. However, due to the addition of extra actuators, greatly increasing the weight, volume, and complexity of the system is unavoidable. This condition is not conducive to the implementation of VSA principle

**Table 1** Overview of prevalent dexterous hands

Hands	Force/N	Driven mechanism	Actuator	Numbers of			
				Fingers	Finger joints	DOFs	Actuators
Utah/MIT hand	–	Tendon	Cylinder	4	16	16	32
Stanford/JPL hand	–	Tendon	Motor	3	9	9	12
DLR hand II	30	Gear, tendon	Motor	4	16	12	12
Shadow hand [17]	–	Tendon	Pneumatic muscle	5	22	18	36
Gifu hand III [18]	2.8	Gear, linkage	Motor	5	20	16	16
DLR/HIT hand II	10	Gear, tendon	Motor	5	20	15	15
UB hand IV [19]	–	Tendon	Motor	5	20	20	25
DEXHAND [20]	25	Tendon	Motor	4	16	12	12
Awiwi hand [21]	20–30	Tendon	Motor	5	21	20	39
R2 hand	22.5	Tendon, linkage	Motor	5	18	12	16
Sandia hand [22]	10	Tendon	Motor	4	12	12	12
SVH hand [23]	–	Gear, linkage	Motor	5	20	20	9
CEA hand [24]	4.2	Tendon, linkage	Motor	5	22	18	18
MagLinkage hand	6.2	Magnetic gear, gear	Motor	3	8	8	8
THU hand [25]	–	Tendon	Motor	5	16	12	12
FLLEX hand [26]	40	Tendon	Motor	5	20	12	12

in dexterous hands with very strict weight and volume requirements. The design of the VSA-based finger mechanism is elaborate in this section. A differential mechanism is adopted in the connection between the finger links and the two actuation units to enable the two actuators to form antagonism in variable stiffness joint (VSJ) mode or form collaboration in series elastic joint (SEJ) mode. Moreover, fingers are more energy-efficient than conventional antagonistic VSAs.

### 2.1 VSA principle

Passive compliance of mechanical systems can be implemented by damping or elastic mechanisms. Compliance through elastic mechanisms is a reliable and widely used method of compliance for mechanical systems. Typical forms are the series elastic actuator (SEA) and the VSA, and the VSA principle is introduced as follows.

Compared with SEA, VSA can actively adjust mechanical stiffness and potential energy to satisfy various task requirements. For a decelerated flexible mechanical system, the part between the actuation side and the load side can be regarded as a coupling block to transmit forces and movements, as shown in Fig. 1. When a generalized force  $F(\phi)$  is exerted to the actuation frame, a generalized actuation frame deflection  $x$  and a generalized load frame deflection  $q$  are obtained until  $F(\phi)$  is balanced with the generalized force  $F_{\text{ext}}$  at the

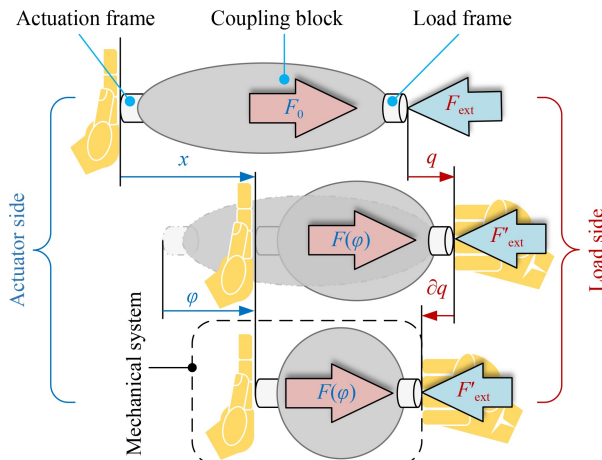


**Fig. 1** Schematic of a flexible mechanical system.

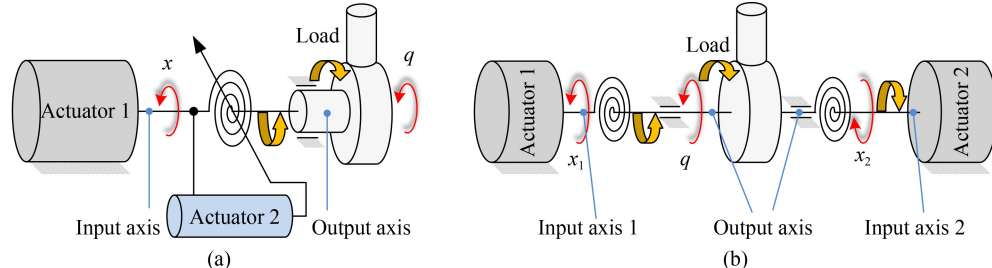


**Fig. 2** Two configurations of VSA. (a) Series VSA, (b) antagonism VSA.

load frame. The transmission stiffness  $k_T$  of the coupling block is defined by

$$k_T(\phi) = \frac{\partial F(\phi)}{\partial \phi}, \quad (1)$$

where  $\phi$  is the compliant deflection, and  $\phi = x - q$ . The actuation source and the coupling block constitute a flexible mechanical system, and its stiffness  $k_{\text{sys}}$  is defined by

$$k_{\text{sys}}(\phi) = -\frac{\partial F(\phi)}{\partial q} = \frac{\partial F_{\text{ext}}}{\partial q}. \quad (2)$$

**Figure 2** depicts two main configurations of VSA: antagonism and series. The series-VSA uses an active nonlinear elastic mechanism to connect actuator 1 with the load side. The driving force is generated by actuator 1, and the secondary actuator 2 adjusts the stiffness of the nonlinear elastic mechanism by adjusting the lever arm or preloading the nonlinear spring mechanisms [27–33] (as shown in Fig. 2(a)). The disadvantage of this method is that actuator 2 does not participate in the torque output of VSA with more additional weight and size, and the energy utilization rate is low. In the antagonistic-VSA (as shown in Fig. 2(b)), the load is connected with two actuators through two nonlinear elastic mechanisms [34,35]. The two actuators exert preload on the elastic elements in advance to change the balance state of the two nonlinear elastic mechanisms, leading to the ability of active joint stiffness variation. The disadvantage of this method is that two actuators are used to drive one-degree of freedom (1-DOF), which increases the complexity of the system. For example, in the DLR hand arm system [36], only a 19-DOF hand is driven by 38 actuators, greatly increasing the cost and complexity of the system.

The stiffness of human body joints is regulated differently to different types of operations, as illustrated in Fig. 3. Case 1 in Fig. 3(a): Stirring a cup of liquid with a finger by the motion of the metacarpophalangeal (MCP) joint while the distal interphalangeal (DIP) and proximal interphalangeal (PIP) joints of the finger are completely abducted. Case 2 in Fig. 3(b): Punching with elbow joint locked at 90° to increase arm stiffness, and the fist is driven by the movement of the shoulder to increase the power of the strike. Case 3 in Fig. 3(c): Most finger joints are adducted and locked to increase the stiffness of

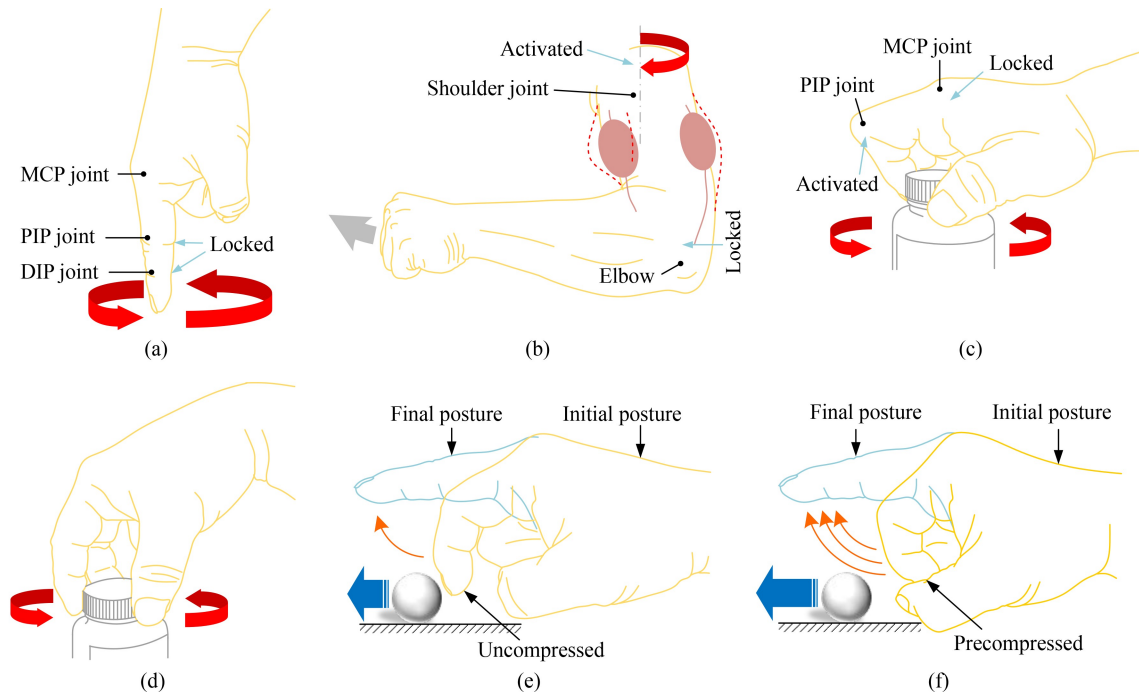


**Fig. 3** Active human body stiffness variations in different manipulations. (a) Finger stirring with DIP joint and PIP joint fully abducted to achieve higher finger stiffness, (b) punching with elbow joint locked at  $90^\circ$  to increase arm stiffness, (c) finger stiffness is increased by adducting finger joints to resist static friction in the tight phase of cap screwing, (d) more finger joints are abducted, and their stiffness decrease in the loose phase of cap screwing, (e) filliping without energy storage, and (f) filliping with energy storage.

fingers and cope with the large friction resistance at the beginning of screwing to tighten a bottle cap. Case 4 in Fig. 3(d): More finger joints are abducted as the cap becomes looser. Case 5 in Fig. 3(e): A finger fillips a ball on the horizontal workbench without energy storage. Case 6 in Fig. 3(f): A finger fillips the same ball on the horizontal workbench with energy storage. In case 1, the finger requires higher joint stiffness to improve the system bandwidth to increase the motion following the fingertip ability. Comparing cases 2, 3, and 4, the human body requires higher joint stiffness to improve the force gain of the end effector in cases 2 and 3, whereas the human body loosens the muscles to reduce the joint stiffness in case 4, thereby reducing energy consumption and muscle and joint injury. Comparing cases 5 and 6, energy storage in the muscles greatly increases the speed and power of the finger movement. These cases indicate that a human will increase body stiffness at the expense of a part of the joint mobilities when performing heavy or precise manipulations and decrease body stiffness to increase the joint mobilities when performing light or imprecise manipulations. Moreover, the energy storage capacity of muscles is very excellent and effective in enhancing the dynamic performance of the body.

## 2.2 Mechanical implementation of VSA principle in the finger system

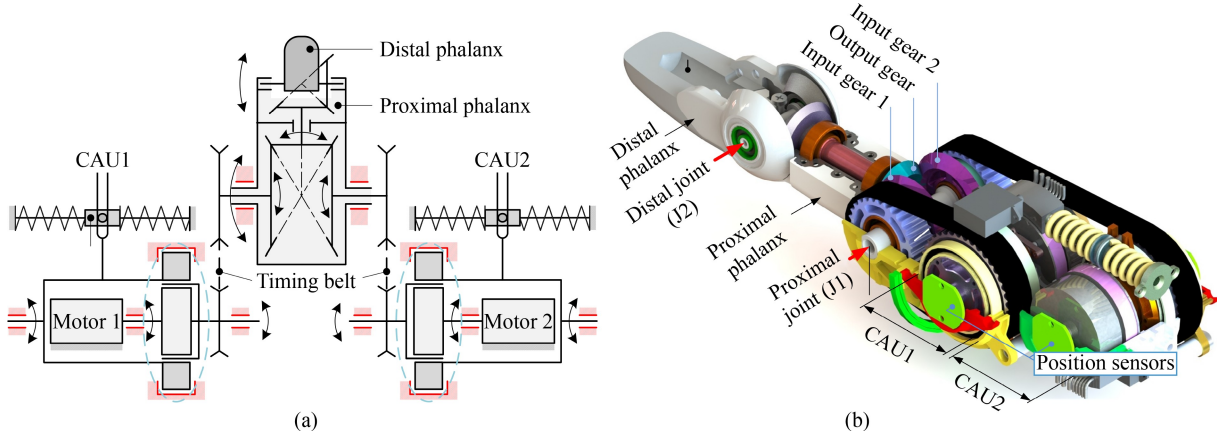
The finger is required to be sufficiently robust against

physical impacts, compact, light-weight, and easily manufactured and maintained. More detailed indicators are shown in Table 2, and the detailed mechanical implementation of the finger is elaborated.

The original motivation of VSA principle is to ensure the safety of the mechanical system. Therefore, a compromise method is implemented by sacrificing a part of the finger DOFs to adjust the finger joint stiffness. This method not only enables the finger to actively adjust its joint stiffness and potential energy, but also avoids the disadvantage of the large size of VSAs. Based on the principle of mechanical passive compliance, a two-joint (J1 and J2) antagonistic variable stiffness dexterous finger is developed, as shown in Fig. 4. For ease of manufacture and assembly, the finger mechanism is designed in three modules: two compliance actuation unit (CAU) mechanisms and a finger joint differential mechanism. The finger joint differential mechanism consists of an input gear 1, an input gear 2, an output gear, and the proximal phalanx, as shown in Fig. 4(a). The driving forces of the two CAUs are transferred from the synchronous belt to the two input gears. Input gear 1 and input gear 2 are used as two sun wheels, the output gear as planetary wheel, and the proximal phalanx as planetary frame, forming a differential mechanism. Moreover, the rotation of the output gear drives the distal phalanx. This variable stiffness method integrates VSAs excellently into the robot finger and reduces the number of actuators, thereby avoiding the disadvantages of VSAs,

**Table 2** Primary physical design goals of the mechanical finger

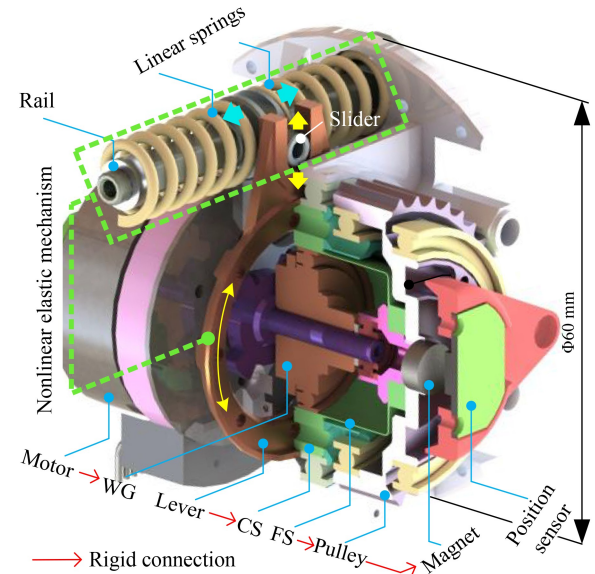
Design values	Criteria
Fingertip force	The finger should be sufficiently strong; the maximum fingertip force is not less than 30 N
Compliant deflection range	The maximum compliant deflection angle of each finger joint is not less than 20°
Weight and volume	The finger mechatronic system should be highly integrated to accommodate the compact size of the dexterous hand
Number of actuators	The ratio of the number of actuators to the DOFs of the actuated joint is not more than 2
Finger kinematics configuration	The finger kinematics configuration can achieve dexterous manipulation ability of the hand

**Fig. 4** Mechanical system of the AVS finger. (a) Sectional view of the finger CAD model, and (b) sketch of the finger mechanism.

such as large size and system complexity, and increases the system reliability.

CAU is mainly composed of motor, circular spline (CS), flexspline (FS), wave generator (WG), and nonlinear elastic mechanism, as shown in Fig. 5. When the FS is subjected to external load, the slider prevents the rigid wheel from deflecting until the torque synthesized by spring forces and the CS torque are in equilibrium. The relationship between CS torque and CS deflection is nonlinear because the force action point moves on the lever. The nonlinear elastic mechanism plays two main roles in CAU: storing kinetic energy as potential energy and acting as flexible connection between actuator and base to bear external load directly. Only the stiffness of the nonlinear elastic mechanism is variable that is related to the deformation of the elastic element and can be varied by changing the precompression of the elastic element, whereas the stiffness of the linear elastic mechanism is immutable. The combination of linear springs and nonlinear mechanism can be used to obtain nonlinear elastic mechanism stiffness.

The finger joint differential mechanism not only achieves the difference between the 2-DOF rotations of the two finger joints with parallel axes, but also enables the finger joint stiffness to be variable by loading each other between two CAUs without any additional actuators. Figure 6(a) depicts the SEJ mode: CAUs operate as nonlinear SEAs and collaborate with each other to drive finger joints when both phalanxes are not obstructed. The torques of the two CAUs flow through the finger joint

**Fig. 5** Sectional view of CAU.

differential mechanism to the two finger joints, and the differential between CAU1 and CAU2 drives the movement of J1 and J2. Figure 6(b) depicts the VSJ mode: The finger operates on the principle of VSA when J1 or J2 is obstructed by internal mechanical limitations or objects grasping at motionless state. The torque applied by CAU2 to the input gear 2 is delivered through the output gear to the input gear 1 and eventually becomes an additional load to CAU1, causing CAU1 and

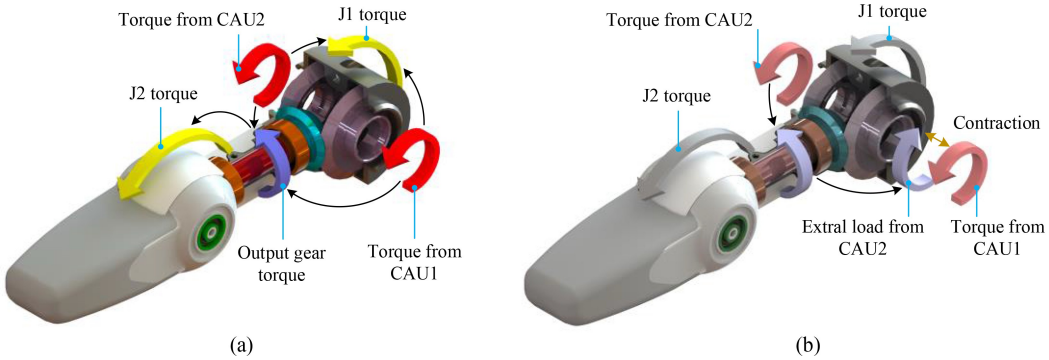


**Fig. 6** Finger operating mode switches between SEJ and VSJ modes. (a) SEJ mode and (b) VSJ mode.

CAU2 to be pre-compressed and vice versa. The pre-compression of the two CAUs' nonlinear elastic mechanisms is controllable and ultimately synthesizes the ability of the finger joint stiffness to vary.

### 3 Finger mathematical modeling

In this section, the kinematics, joint stiffness, and potential energy of the finger are derived and are finally used as the basis for finger stiffness variation.

Passive compliance by appending elastic elements to mechanical systems can excellently solve collision problems. However, it can also cause inaccuracies and delays in the finger system. An accurate model of finger should be built to accurately control finger movement. Building this model is very difficult because of the flexibility of synchronous belt and shaft parts. By comparison, the springs are much softer than other parts in the finger mechanism. Therefore, spring-dominated compliance should be considered primarily. The moment of the finger joint is synthesized by the moment of two CAUs. Different CAU stiffness and finger joint stiffness are responded when the finger is subjected to different external forces due to the nonlinearity of CAU stiffness. In this section, the mathematical model between the external loads of the upper finger and the CAU torques is described by establishing the Jacobian of the finger, and then the corresponding stiffness of the finger joint is solved, thereby providing the basis for the finger operating strategy.

#### 3.1 Kinematics and dynamics

Figure 7 depicts the Denavit–Hartenberg model and the two CAU kinematics models.

The equation for converting CAU output axis rotations to finger joint abduction/adduction angles is as follows:

$$\begin{bmatrix} \theta_1 \\ \theta_2 \end{bmatrix} = \mathbf{T}_K \begin{bmatrix} q_1 \\ q_2 \end{bmatrix}, \quad (3)$$

where  $\theta_1$  and  $\theta_2$  are the angular positions of J1

abduction/adduction and J2 abduction/adduction, respectively,  $q_1$  and  $q_2$  are the angular positions of CAU1 output shaft and CAU2 output shaft, respectively, and  $\mathbf{T}_K$  is the transformation matrix of forward joint kinematics and non-singular.  $\mathbf{T}_K = \begin{bmatrix} 1 & -1 & 1 & 1 \\ 2p_a & 2p_a & 2p_a p_b & 2p_a p_b \end{bmatrix}$ , where  $p_a$  and  $p_b$  are the transmission ratios of synchronous belt and differential gear, respectively.

The equation for converting CAU output torques to finger joint torques is as follows:

$$\begin{bmatrix} \tau_1 \\ \tau_2 \end{bmatrix} = \mathbf{T}_D \begin{bmatrix} \tau_{CAU1} \\ \tau_{CAU2} \end{bmatrix}, \quad (4)$$

where  $\tau_1$  and  $\tau_2$  are J1 torque and J2 torque, respectively,  $\mathbf{T}_D = (\mathbf{T}_K^{-1})^T$ , and  $\mathbf{T}_D$  is the transformation matrix of forward joint dynamics and non-singular.

#### 3.2 Finger joint stiffness modeling

In this section, the finger joint stiffness model is established. Figure 8 depicts the circular spline of the  $i$ th ( $i = 1, 2$ ) CAU in the deflected position. In the  $i$ th ( $i = 1, 2$ ) CAU, an external load exerted on the finger causes such equilibrium as

$$\begin{cases} F_{si} = (F_{0i} + K_s \Delta x_{si}) - (F_{0i} - K_s \Delta x_{si}) = 2K_s \Delta x_{si}, \\ \tau_{CSi} = 2K_s R^2 \tan \theta_{CSi}, \end{cases} \quad (5)$$

where  $F_{si}$ ,  $F_{0i}$ ,  $\Delta x_{si}$ ,  $K_s$ ,  $\theta_{CSi}$ ,  $\tau_{CSi}$ , and  $R$  are the resultant spring force on the slider, the initial spring force, the deflection of the slider, the stiffness of linear spring, the angular displacement of CS, CS torque, and the distance between the CS axis and the slider routine, respectively.

In Eq. (5),  $\Delta x_{si} = R \tan \theta_{CSi}$ . The maximum CS deflection angle is designed to be  $20^\circ$ . To ensure that the spring forces of spring 1 and spring 2 do not vanish within the effective deflection range of CS,  $F_{0i} > 3^{-0.5} K_s R$  is required.

According to Eq. (2), the  $i$ th CAU's  $x$ ,  $q$ , and  $F(\varphi)$  are the motor side displacement  $\theta_{Mi}$ , where  $\theta_{Mi} = \theta_{mi}/N$ , the FS angular displacement  $q_i$ , and the driving torque of the pulley  $\tau_{CAUi}$ , respectively.  $\theta_{mi}$  and  $N$  are the angular

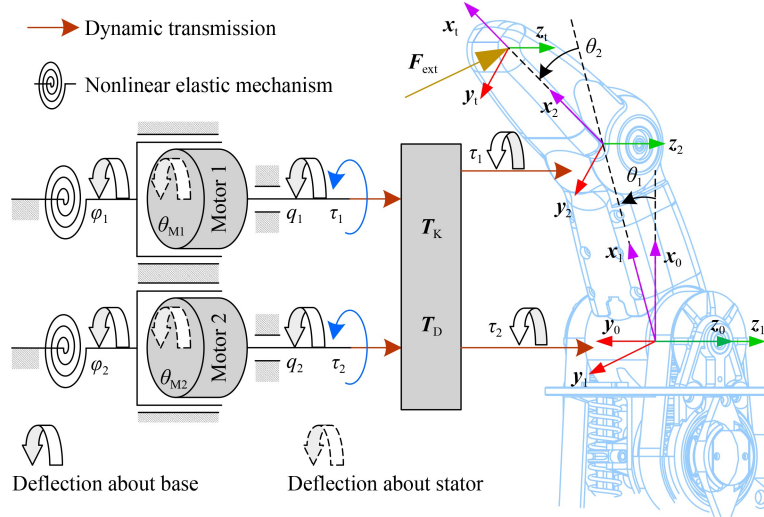


Fig. 7 Kinematics models of finger links and CAUs.

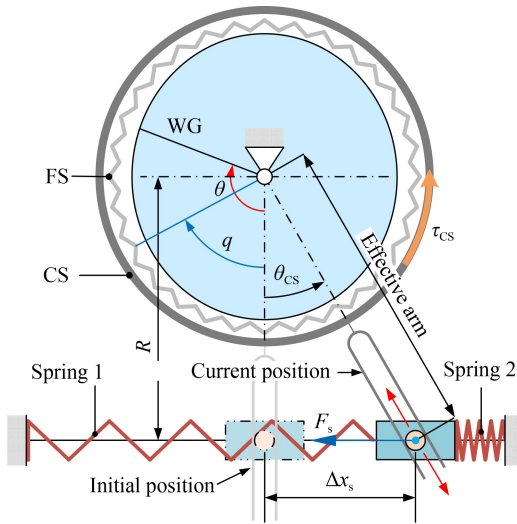


Fig. 8 Circular spline in deflected position.

displacement of motor and the deceleration ratio of the harmonic drive gear, respectively. The following force and motion transfer relationships among CS, FS, and WG are obtained according to harmonic drive principle.

$$\begin{cases} \theta_{WG} = (N+1)\theta_{CS} - N\theta_{FS}, \\ \tau_{FS} = -\frac{N}{N+1}\tau_{CS}, \end{cases} \quad (6)$$

where  $\theta_{CS}$ ,  $\theta_{FS}$ , and  $\theta_{WG}$  are the angular deflections of CS, FS, and WG, respectively, and  $\tau_{CS}$  and  $\tau_{FS}$  are CS torque and FS torque, respectively. Hence, the expressions of  $q_i$ ,  $\varphi_i$ , and  $\tau_{CAUi}$  are presented as follows:

$$\begin{cases} q_i = \frac{N-1}{N}\theta_{CSi} + \frac{1}{N}\theta_{mi}, \\ \varphi_i = \theta_{Mi} - q_i = -\theta_{CSi}, \\ \tau_{CAUi}(q_i, \theta_{Mi}) = -\frac{N}{N+1}\tau_{CSi} = 2K_sR^2 \tan \varphi_i. \end{cases} \quad (7)$$

Based on the definition of mechanical stiffness in Eq. (2), the stiffness of the  $i$ th CAU can be obtained as follows:

$$K_{CAUi} = -\frac{\partial \tau_{CAUi}(q_i, \theta_{Mi})}{\partial q_i} = 2K_sR^2 \cos^{-2}(\theta_{Mi} - q_i). \quad (8)$$

For nonlinear elastic mechanisms, different  $\varphi$  corresponds to different stiffness values. The  $\varphi_i$  and the stiffness of the  $i$ th CAU are determined by the load on its pulley. The characteristic between the external load and  $\varphi_i$  of the  $i$ th CAU and that between the stiffness and  $\varphi_i$  of the  $i$ th CAU are shown in Figs. 9(a) and 9(b), respectively. Adjusting the  $i$ th CAU stiffness requires varying its  $\varphi_i$ . However, a variation of its driving torque is caused at the same time. Therefore, adjusting the stiffness of a CAU actively requires an additional torque to be applied by another. For a fixed stiffness (stiffness value is constant) mechanical device, the mechanical stiffness is independent of compliant deflection even if the external load changes in anyway.

The joint differential mechanism couples the motion of two output shafts of CAU to synthesize the motion of two finger joints. Therefore, the  $i$ th finger joint torque  $\tau_{Ji}$  is a function of  $\varphi_1$  and  $\varphi_2$ ; thus,  $\tau_{Ji}$  can be calculated via position vector  $\Theta$  ( $i = 1, 2$  and  $\Theta = [q_1 \ q_2 \ \theta_{M1} \ \theta_{M2}]^T$ ). Based on the definition of mechanical stiffness in Eq. (2), the expression of the  $i$ th finger joint stiffness ( $K_{Ji}$ ) is given by the following:

$$K_{Ji} = -\frac{\partial \tau_{Ji}}{\partial \theta_i}. \quad (9)$$

The  $i$ th ( $i = 1, 2$ ) CAU output torque based on position vector is obtained as follows:

$$\begin{aligned} \tau_{CAUi}(\Theta) &= 2K_sR^2 \tan(\theta_{Mi} - q_i) \\ &= 2K_sR^2 \tan(\theta_{Mi} + (-1)^i p_a \theta_1 - p_b \theta_2). \end{aligned} \quad (10)$$

According to Eqs. (4) and (10), the finger joint torque

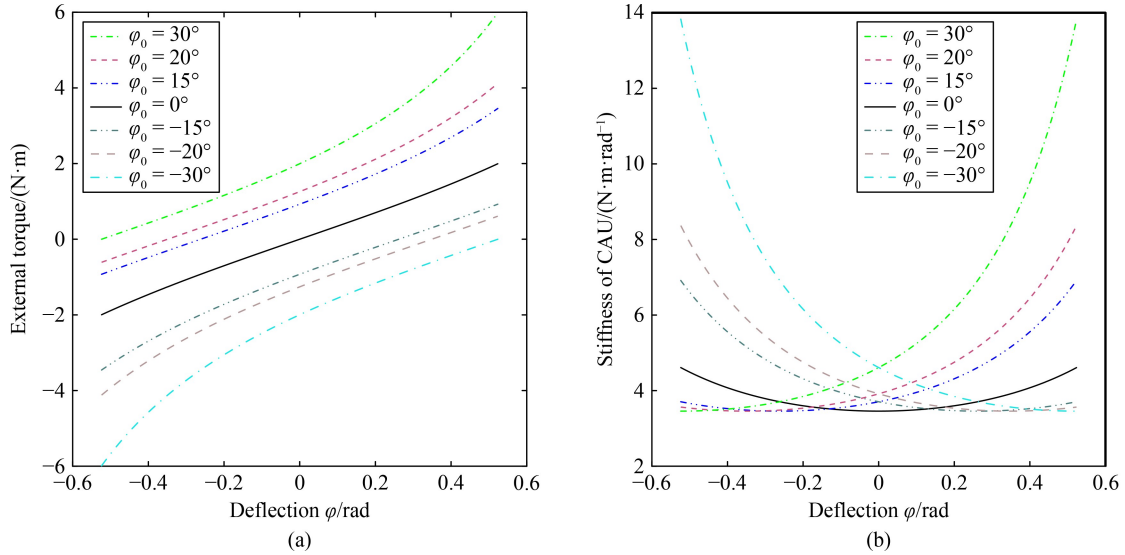


**Fig. 9** Characteristics of CAU. (a) External load of CAU versus compliance deflection at different pre-compressions and (b) CAU stiffness versus compliance deflection at different pre-compressions.

vector  $\tau_J$  ( $\tau_J = [\tau_{J1} \ \tau_{J2}]^T$ ) based on the position vector is obtained as follows:

$$\tau_J(\Theta) = 2K_s R^2 T_D \begin{bmatrix} \tan(\theta_{M1} - p_a \theta_1 - p_b p_a \theta_2) \\ \tan(\theta_{M2} + p_a \theta_1 - p_b p_a \theta_2) \end{bmatrix}. \quad (11)$$

According to Eq. (2), the finger joint stiffness vector  $K_J$  ( $K_J = [K_{J1} \ K_{J2}]^T$ ) based on position vector is obtained as follows:

$$\begin{aligned} K_J(\Theta) &= 2K_s R^2 T_D \begin{bmatrix} p_a \cos^2(\theta_{M1} - p_a \theta_1 - p_b p_a \theta_2) \\ p_a p_b \cos^2(\theta_{M2} + p_a \theta_1 - p_b p_a \theta_2) \end{bmatrix} \\ &= 2K_s R^2 T_D \begin{bmatrix} p_a \cos^2(\theta_{M1} - q_1) \\ p_a p_b \cos^2(\theta_{M2} - q_2) \end{bmatrix}. \end{aligned} \quad (12)$$

The method of deriving finger joint stiffness from position information is described in the previous section. This method is convenient to observe finger stiffness in real time because the position information is easy to measure. However, it involves many variables, which is not conducive to analyzing the variation law of joint stiffness. A functional relationship exists between a mechanical stiffness and its external load. Thus, the mechanical stiffness can be characterized by force information, which facilitates the analysis of stiffness variation; it is also applicable to CAU and finger joints. CAU stiffness and finger joint stiffness based on force information can be solved using a concept called eigen triangle. Eigen triangle is a convenient analysis tool with triangular function characteristics and can be applied to force analysis of various mechanisms, especially in finger mechanisms with complex linear coupling. In the  $i$ th CAU, an eigen triangle is a right triangle with a bottom length of  $2K_s R^2$  and a height of  $\tau_{CAUi}$ . The sharp angle between the bottom edge and the inclined edge is only  $\varphi_i$  ( $i = 1, 2$ ), as shown in Fig. 10.

Using the eigen triangle, the force-based CAU stiffness

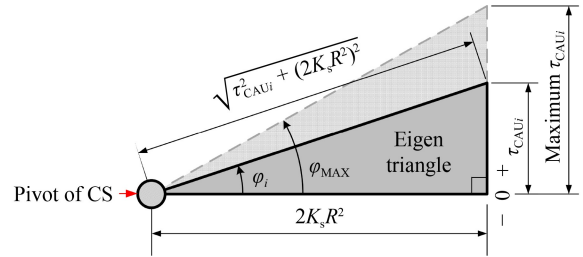


**Fig. 10** Eigen triangle of the CAU statics model.

( $K_{CAUi}$ ) is given by the following:

$$K_{CAUi}(\tau_{CAUi}) = 2K_s R^2 \cos^2 \varphi = \frac{\tau_{CAUi}^2}{2K_s R^2} + 2K_s R^2. \quad (13)$$

Equation (13) shows that the stiffness of CAU follows a quadratic variation law. The  $i$ th finger joint stiffness based on force ( $\tau_J = [\tau_{J1} \ \tau_{J2}]^T$ ) is given by the following:

$$K_{Ji}(\tau_J) = 2p_a^2 p_b^{2(i-1)} K_s R^2 \left( \sum_{i=1}^2 \left( \frac{\tau_{CAUi}}{2K_s R^2} \right)^2 + 2 \right). \quad (14)$$

According to Eq. (14), the J1 stiffness characteristic versus  $\tau_{CAUi}$  and  $\tau_{CAU2}$  is revealed in Fig. 11(a), and the J2 stiffness characteristic versus  $\tau_{CAUi}$  and  $\tau_{CAU2}$  is revealed in Fig. 11(b).

### 3.3 Potential energy

Potential energy can be calculated by integrating forces into positions, but this method is very complex to implement in the finger.

$$\begin{aligned} E_{CAUi}(\varphi_i) &= \int_0^{\varphi_i} \tau_{CAUi} d\varphi_i = -2K_s R^2 \ln |\cos \varphi_i| \\ &= -2K_s R^2 \ln |\cos (\theta_{Mi} - q_i)|. \end{aligned} \quad (15)$$

Using the eigen triangle, the  $i$ th CAU potential energy versus its output torque can be obtained as follows:

$$E_{\text{CAUi}}(\tau_{\text{CAUi}}) = -2K_s R^2 \ln \frac{2K_s R^2}{\sqrt{\tau_{\text{CAUi}}^2 + (2K_s R^2)^2}}. \quad (16)$$

However, using position information to solve the potential energy of the entire finger requires a very complex integral operation. Hence, the eigen triangle plays an effective role in the calculation of finger potential energy. Using the Eigen triangle, the finger potential energy  $E_{\text{finger}}(\tau)$  based on force information can be obtained as follows:

$$E_{\text{finger}}(\tau) = 2K_s R^2 \left( -\sum_{i=1}^2 \ln \frac{2K_s R^2}{\sqrt{\tau_{\text{CAUi}}^2 + (2K_s R^2)^2}} \right). \quad (17)$$

According to Eq. (17), the finger potential energy versus  $\tau_{\text{CAU1}}$  and  $\tau_{\text{CAU2}}$  is revealed in Fig. 11(c).

### 3.4 Changing the finger joint stiffness

Robot fingers should be sufficiently soft to reduce system bandwidth in case of physical impacts to ensure finger

system safety, but finger accuracy is decreased under this condition. The adjustment strategy of finger joint stiffness is proposed in this section.

When dexterous hands perform higher-precision operations in sufficiently safe environments, higher finger stiffness is required to improve system bandwidth. Without changing the external load, the adjustment of finger stiffness can be achieved by sacrificing one DOF joint mobility of the finger and switching the finger to VSJ mode through antagonistic motion of two CAUs. The finger stiffness adjusting mode can be divided into distal-joint-locked stiffness adjusting (DSA) mode and proximal-joint-locked stiffness adjusting (PSA) mode by the locked joint, as shown in Fig. 12.

#### 1) DSA mode

In DSA operating mode, the distal phalanx is fully abducted or adducted to the J2 mechanical limitation, whereas J1 is mobile, and its stiffness can be actively adjusted.

Case 1: When  $\tau_{\text{CAU1}} = \tau_{\text{CAU2}} < 0$ ,  $\tau_{\text{J1}} = 0$ ,  $\tau_{\text{J2}} < 0$ , and  $q_1 - \theta_{M1} = q_2 - \theta_{M2} > 0$ , J2 will be fully abducted to its negative mechanical limitation,  $\theta_2 = -45^\circ$ . According to the joint differential principle,  $q_1 + q_2 = -0.5i_a i_b \pi$ .

The stiffness vector of J1 and J2 is obtained as follows:

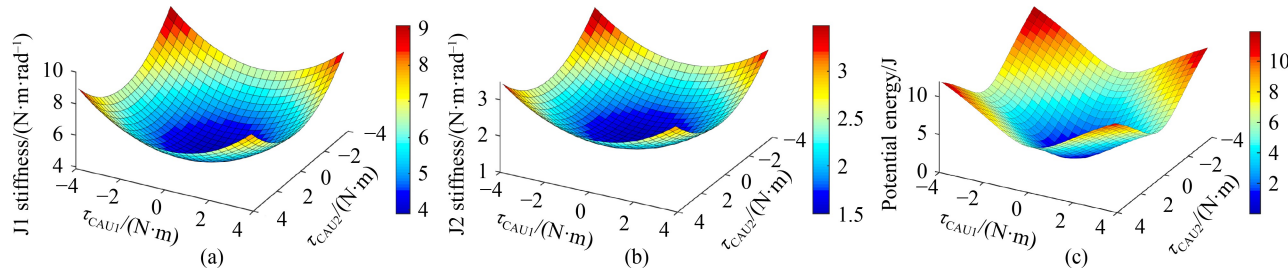


**Fig. 11** Simulation results of the finger model. (a) J1 stiffness versus  $\tau_{\text{CAU1}}$  and  $\tau_{\text{CAU2}}$ , (b) J2 stiffness versus  $\tau_{\text{CAU1}}$  and  $\tau_{\text{CAU2}}$ , and (c) finger potential energy versus  $\tau_{\text{CAU1}}$  and  $\tau_{\text{CAU2}}$ .

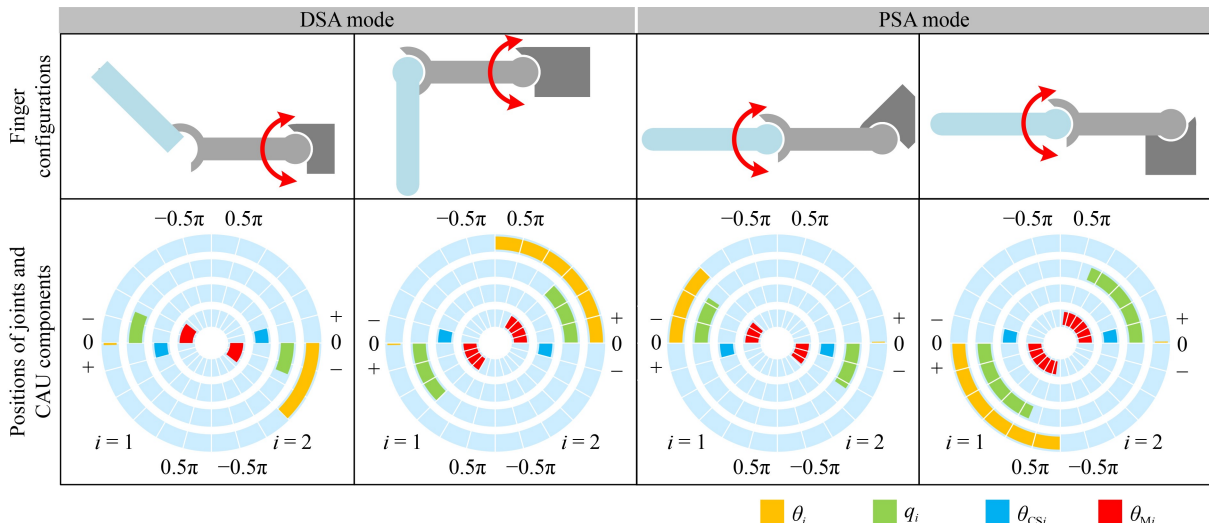


**Fig. 12** Positions of the  $i$ th finger joint and the harmonic gear components of the  $i$ th CAU in different stiffness adjusting modes.

$$\begin{bmatrix} K_{J1} \\ K_{J2} \end{bmatrix} = \begin{bmatrix} 4p_a^2 K_s R^2 \cos^2(q_1 - \theta_{M1}) \\ \infty \end{bmatrix}. \quad (18)$$

Case 2: When  $\tau_{CAU1} = \tau_{CAU2} > 0$ ,  $\tau_{J1} = 0$ ,  $\tau_{J2} > 0$ , and  $q_1 - \theta_{M1} = q_2 - \theta_{M2} < 0$ , J2 will be fully adducted to its positive mechanical limitation,  $\theta_2 = 90^\circ$ . According to the joint differential principle,  $q_1 + q_2 = i_a i_b \pi$ .

The stiffness vector of J1 and J2 is obtained as follows:

$$\begin{bmatrix} K_{J1} \\ K_{J2} \end{bmatrix} = \begin{bmatrix} 4p_a^2 K_s R^2 \cos^2(q_1 - \theta_{M1}) \\ 4p_a^2 p_b^2 K_s R^2 \cos^2(q_1 - \theta_{M1}) \end{bmatrix}. \quad (19)$$

## 2) PSA mode

In PSA mode, the proximal phalanx is fully abducted or adducted to J1 mechanical limitation, whereas J2 is mobile, and its stiffness can be actively adjusted.

Case 1: When  $\tau_{CAU1} + \tau_{CAU2} = 0$  and  $\tau_{CAU2} < 0 < \tau_{CAU1}$ ,  $\tau_{J2} = 0$ ,  $\tau_{J1} > 0$ , and  $q_1 - \theta_{M1} = \theta_{M2} - q_2 < 0$ , J1 will be fully adducted to its positive mechanical limitation,  $\theta_1 = 90^\circ$ . According to the joint differential principle,  $q_1 - q_2 = i_a \pi$ .

The stiffness vector of J1 and J2 is the same as Eq. (19).

Case 2: When  $\tau_{CAU1} + \tau_{CAU2} = 0$  and  $\tau_{CAU1} < 0 < \tau_{CAU2}$ ,  $\tau_{J1} < 0$ ,  $\tau_{J2} = 0$ , and  $q_1 - \theta_{M1} = \theta_{M2} - q_2 > 0$ , J1 will be fully abducted to its negative mechanical limitation,  $\theta_1 = -45^\circ$ . According to the joint differential principle,  $q_1 - q_2 = -0.5i_a \pi$ .

$$\begin{bmatrix} K_{J1} \\ K_{J2} \end{bmatrix} = \begin{bmatrix} \infty \\ 4p_a^2 p_b^2 K_s R^2 \cos^2(q_1 - \theta_{M1}) \end{bmatrix}. \quad (20)$$

## 4 Experiments

A finger prototype weighing 480 g was fabricated with alloy material and 3D printed material. The prototype and its controller hardware are shown in Fig. 13. A compact, lightweight harmonic gear and a Faulhaber BXT external rotor brushless direct current motor are adopted in each CAU that can provide peak torque of up to 4.1 N·m at the CAU output shaft, and the maximum fingertip force reaches up to 40 N. The stiffness of CAU is between 3.45 and 4.6 N·m/rad, and the maximum storable potential energy of a single CAU is 0.5 J. The finger motion is driven by a pair of motors, and its closed loop control is achieved by measuring the position information of the finger via four absolute magnetic encoders (AS5048A) with 14-bit accuracy as feedback. The position sensors at the CAU output side are used as the finger joint feedbacks to realize the closed-loop control of the finger motion, and the networked motion controller is adopted to drive and control the speed of the motor. The PC sends out the motion command of the finger joint, and the STM32 controller calculates the required action of the motor to reach the predetermined position, and then sends the motor motion commands to the motion controller of the network. A proportional plus derivative (PD) controller is adopted for the motion control system of the finger, as shown in Fig. 14. The parameters of the control system are annotated in Table 3.

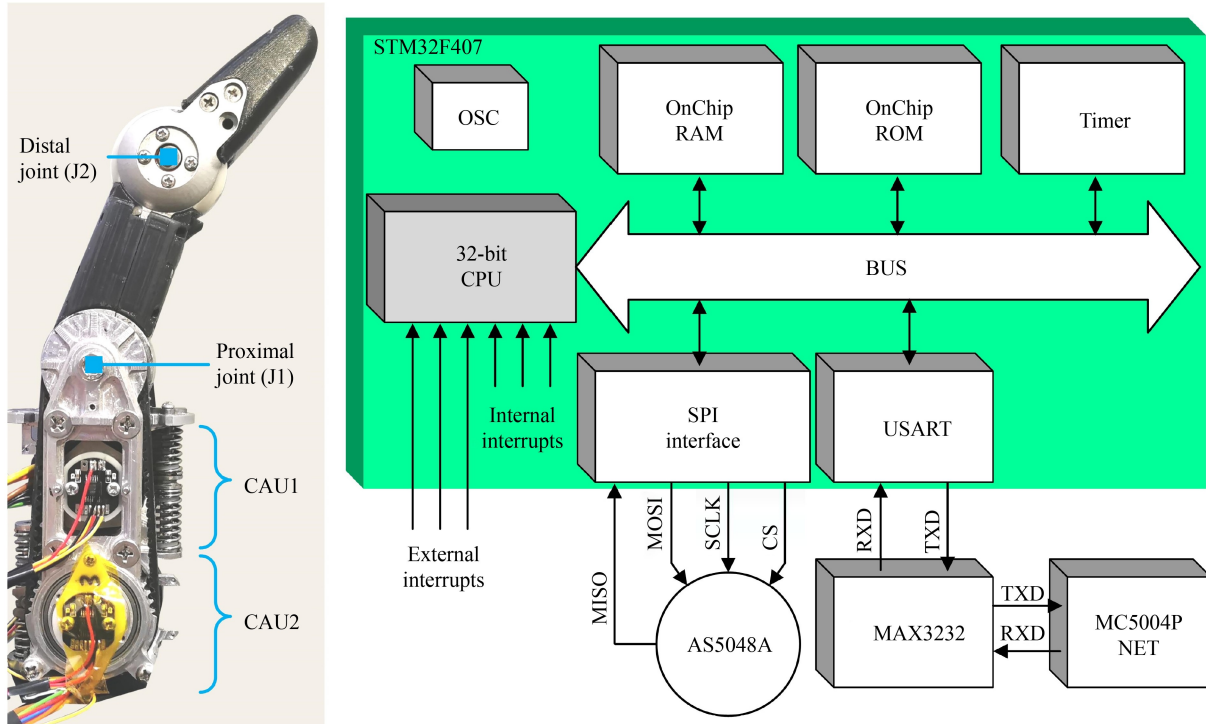


**Fig. 13** Prototype of AVS-finger and its controller hardware.

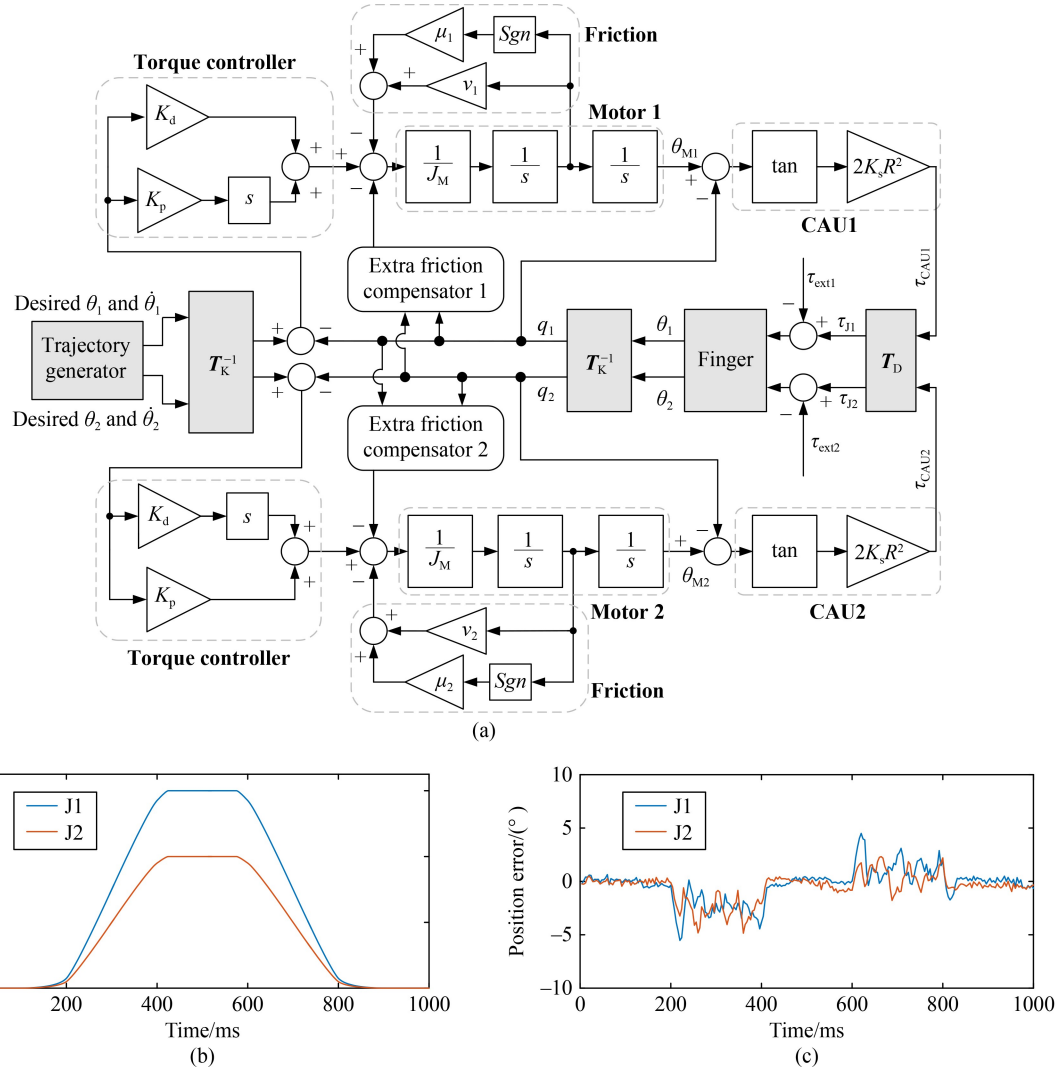


**Fig. 14** Finger motion control system and its control effects. (a) Finger motion control block diagram, (b) desired joint trajectories, and (c) position errors of J1 and J2.

**Table 3** Parameters of finger motion control system

Variables	Notes
\$K_p\$	Proportional gain of the PD controller
\$K_d\$	Differential gain of the PD controller
\$\mu_1, \mu_2\$	Coefficients of coulomb friction of CAU1 and CAU2, respectively
\$\nu_1, \nu_2\$	Coefficients of sliding friction of CAU1 and CAU2, respectively
\$J_M\$	Motor inertia of deceleration

#### 4.1 Loading and robustness tests

The experiment shown in Fig. 15(a) verifies the excellent robustness of the finger mechanism as described in Section 2. Hammering the finger with a 1.5 kg steel hammer in the positive and negative directions of the finger causes no structural damages. Finally, the finger returns to its original position under the action of the motion controller. Figure 15(b) depicts the result of finger loading test. The finger can lift weights of 2 and 4 kg at

the fingertip in a fully straightened configuration without any structural damage or motor abnormalities.

#### 4.2 Grasping and manipulation experiments

To assess the internal manipulation performance of the finger, several grasping and manipulating tests are carried out. Fingertip grasping (or precise grasping) and power grasping tests are performed on a group of typical objects in daily life. Cylindrical objects, rectangular objects, and spherical objects of different sizes are selected to guarantee the universality of finger grasping. Precise grasping tests on a 55 mm × 26 mm × 13 mm cuboid, a 26-mm diameter cylinder, and a 13 mm diameter plastic ball are performed, and power grasping tests on a 55 mm × 55 mm × 55 mm cuboid, a 56-mm diameter cylinder, and a 74-mm diameter apple are performed as shown in Fig. 15(c).

Figure 15(d) depicts the operation of screwing bottle



**Fig. 15** Physical impact, lifting, grasping, and manipulating tests. (a) Hammering the finger with a steel hammer at a speed of 1.2 m/s, (b) lifting tests, (c) precise grasping and power grasping, (d) screwing the cap, and (e) clicking the roller of the mouse.

cap. The cap of the plastic bottle fixed on the workbench is screwed around counterclockwise with the finger. Figure 15(e) depicts the computer mouse manipulation test, in which the roller of the mouse is clicked with the fingertip.

#### 4.3 Joint stiffness identifications

The stiffness characteristics of two finger joints can be identified by the external load on the joint and the corresponding flexibility deflection angle, and the

experimental device is set as shown in Fig. 16. A set of weights of the same weight is suspended and removed one by one at the fingertip with the motor position fixed at  $0^\circ$  to measure the two joint deflections. The deflections of the two joint angles are measured by the two magnetic encoders at the CAU output side. The experimental and model results of J1 and J2 are depicted in Figs. 16(b) and 16(c), respectively. The existing deviations are mainly caused by the difference of friction between J1 and J2, and also by the offset of the origin of force of the suspended weight on the fingertip.

#### 4.4 Joint stiffness variation

The joint stiffness variation experiment is set up with a 200-g weight dropping freely from a position of 0.3-m high hitting the fingertips in DSA-mode finger configuration and PSA-mode finger configuration, respectively, as shown in Fig. 17(a). Larger finger joint stiffness results in smaller joint deflection after physical impact. The change in the joint stiffness can be characterized by the deflection movement of the finger

joint during the impact. In DSA-mode finger configuration, the position of J2 is maintained at  $90^\circ$  all the time, and the fingertip is hit with  $\varphi_1 = \varphi_2 = 0^\circ$ ,  $\varphi_1 = \varphi_2 = 10^\circ$ , and  $\varphi_1 = \varphi_2 = 20^\circ$ . The experimental results shown in Fig. 17(b) reveal that as the modulus of  $\varphi_i$  ( $i = 1, 2$ ) increases, the stiffness of J1 increases as well as the deflection, resulting in a reduction of the peak J1 deflection under the collision. The experimental results are shown in Fig. 17(b). In PSA mode finger configuration, the position of J1 is maintained at  $90^\circ$  all

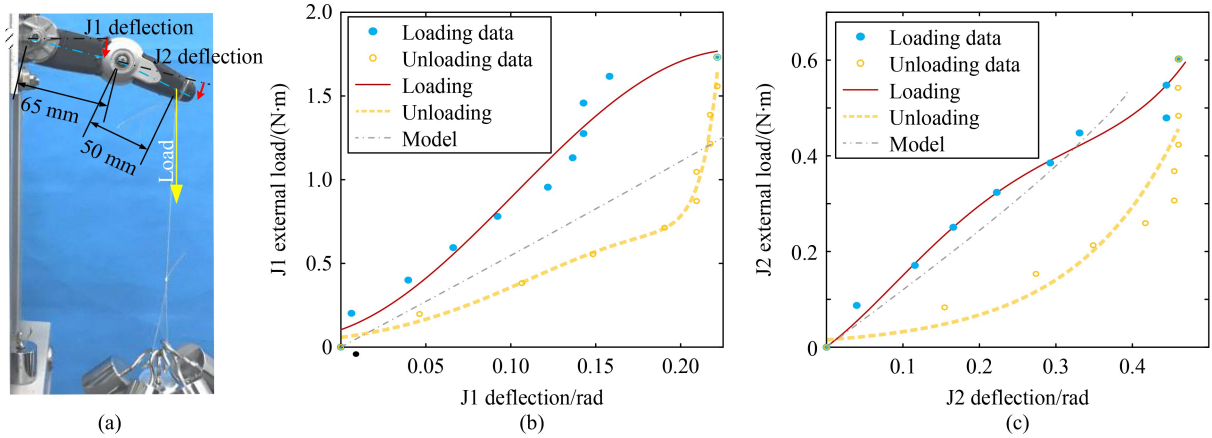


**Fig. 16** Model validation of finger joint stiffness characteristics. (a) Experimental setup; experimental and model results of (b) J1 and (c) J2.

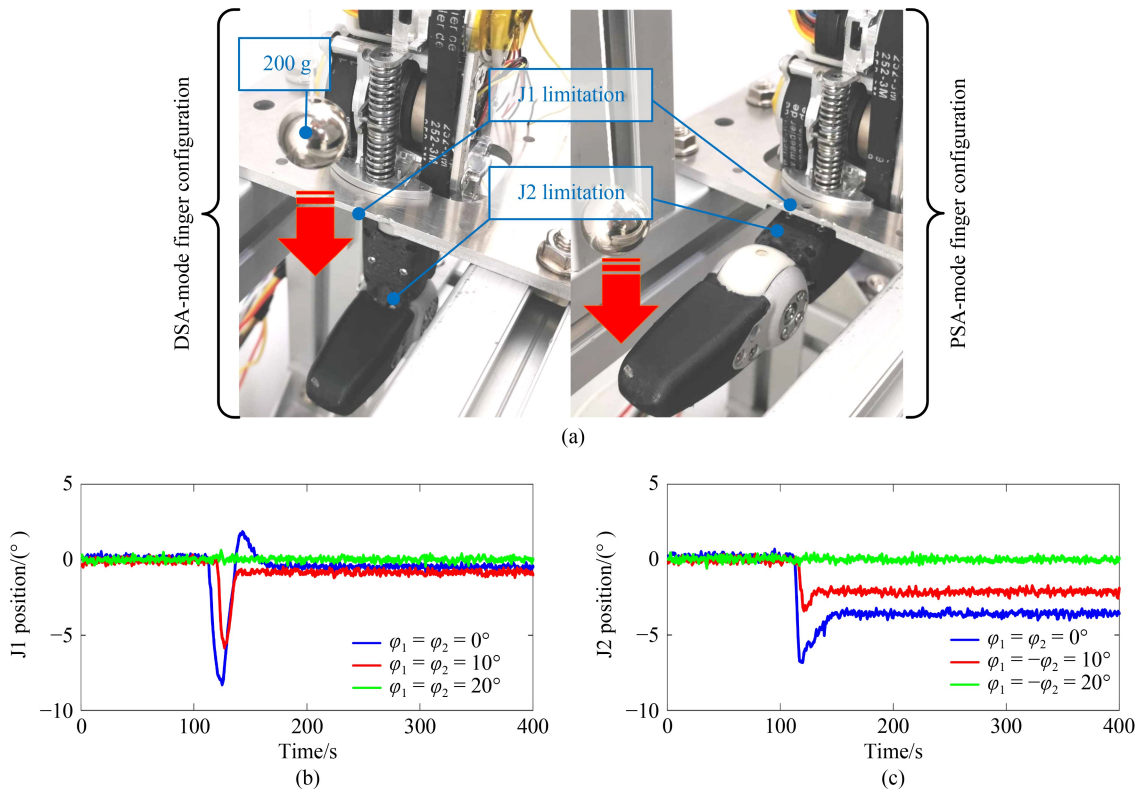


**Fig. 17** Finger joint stiffness adjusting operation tests. (a) Experimental setup; (b) J1 positions and (c) J2 positions during finger impact with different finger stiffness presets.

the time, and the fingertip is hit with  $\varphi_1 = \varphi_2 = 0^\circ$ ,  $\varphi_1 = -\varphi_2 = 10^\circ$ , and  $\varphi_1 = -\varphi_2 = 20^\circ$ . The experimental results shown in Fig. 17(c) reveal that as the modulus of  $\varphi_i$  ( $i = 1, 2$ ) increases, the stiffness of the J2 increases as well as the deflection, resulting in a reduction of the peak J1 deflection under the collision. The experimental results are shown in Fig. 17(b).

## 5 Conclusions and future work

This paper presented a hardware implementation method, modeling, identification, and stiffness adjusting methods of the AVS-finger based on harmonic driven mechanism and VSA principle. The finger mechanism achieves passive submissiveness to physical impacts and implementation of VSA principles in the finger of the dexterous hand in very compact size without adding supernumerary actuators. The mechanical design and stiffness adjusting operation methods of the AVS-finger were elaborated. Biologically inspired by the biomimetic stiffness variation principle of discarding some mobilities to adjust stiffness, the stiffness adjusting operation methods are achieved by switching a finger joint to its mechanical limitation to adjust finger stiffness. The experimental results of joint deflection with finger impact under different finger stiffness presets were provided. The finger was proven to have excellent mechanical robustness by hammering experiments. Through a series of grasping and manipulation experiments, the satisfactory grasping and manipulation ability of the finger was verified.

In future work, optimization of nonlinear elastic mechanisms in the CAU will be implemented to improve stiffness adjustment range and more detailed model evaluation. Furthermore, structural optimization, lubrication, weight reduction, and compactness will be implemented, and the hardware system of a complete dexterous hand will be designed and fabricated.

## Nomenclature

### Abbreviations

AVS	Antagonistic variable stiffness
CAU	Compliant actuation unit
CS	Circular spline
DOF	Degree of freedom
DSA	Distal-joint-locked stiffness adjusting
FS	Flexspline
PD	Proportional plus derivative
PSA	Proximal-joint-locked stiffness adjusting
SEA	Series elastic actuator

SEJ	Series elastic joint
VSA	Variable stiffness actuator
VSJ	Variable stiffness joint
DIP	Distal interphalangeal
PIP	Proximal interphalangeal
WG	Wave generator
<b>Variables</b>	
$E_{CAUi}$	Potential energy
$E_{\text{finger}}$	Finger potential energy
$F(\varphi)$	Generalized force exerted to the actuation frame
$F_{\text{ext}}$	Generalized force at the load frame
$F_{si}, F_{0i}, \Delta x_{si}$	Resultant spring force on the slider, the initial spring force, the deflection of the slider, the stiffness of linear spring
$K_s, \theta_{CSi}, \tau_{CSi}$	, the angular displacement of CS, and CS torque of the $i$ th CAU, respectively
$J_M$	Motor inertia of deceleration
$K_{CAUi}$	Stiffness of the $i$ th CAU
$K_p, K_d$	Proportional gain and differential gain of the PD controller, respectively
$K_{Ji} (i = 1, 2)$	$i$ th finger joint stiffness
$k_{\text{sys}}$	Stiffness of a flexible mechanical system
$k_T$	Transmission stiffness of the coupling block
$\mathbf{K}_J$	Stiffness vector of the finger joints
$N$	Deceleration ratio of the harmonic drive gear
$p_a, p_b$	Synchronous belt transmission ratio and differential gear transmission ratio, respectively
$q$	Generalized load frame deflection
$q_i (i = 1, 2)$	Output shaft angular position the $i$ th CAU
$R$	Distance between the CS axis and the slider routine
$T_D$	Transformation matrix of forward joint dynamics
$T_K$	Transformation matrix of forward joint kinematics
$x$	Generalized actuation frame deflection
$\theta_{CS}, \theta_{FS}, \theta_{WG}$	Angular deflections of CS, FS, and WG, respectively
$\theta_i (i = 1, 2)$	Angular positions of joint $i$ abduction/adduction
$\theta_{mi}$	Angular displacement of motor of the $i$ th CAU
$\theta_{Mi}$	Motor side displacement
$\Theta$	Position vector
$\mu_1, \mu_2$	Coefficients of coulomb friction of CAU1 and CAU2, respectively
$\nu_1, \nu_2$	Coefficients of sliding friction of CAU1 and CAU2, respectively
$\tau_1, \tau_2$	J1 torque and J2 torque, respectively
$\tau_{CAUi}$	Torque
$\tau_{CS}, \tau_{FS}$	CS torque and FS torque, respectively
$\tau_{Ji} (i = 1, 2)$	$i$ th finger joint torque
$\tau_J$	Torque vector
$\varphi$	Compliant deflection

**Acknowledgements** This work was supported by the National Key R&D Program of China (Grant No. 2017YFB1300400), and the Major Research Plan of the National Natural Science Foundation of China (Grant No. 91848202).

**Open Access** This article is licensed under a Creative Commons Attribution 4.0 International License, which permits use, sharing, adaptation, distribution, and reproduction in any medium or format as long as appropriate credit is given to the original author(s) and source, a link to the Creative Commons license is provided, and the changes made are indicated.

The images or other third-party material in this article are included in the article's Creative Commons license, unless indicated otherwise in a credit line to the material. If material is not included in the article's Creative Commons license and your intended use is not permitted by statutory regulation or exceeds the permitted use, you will need to obtain permission directly from the copyright holder.

Visit <http://creativecommons.org/licenses/by/4.0/> to view a copy of this license.

## References

1. Mattar E. A survey of bio-inspired robotics hands implementation: new directions in dexterous manipulation. *Robotics and Autonomous Systems*, 2013, 61(5): 517–544
2. Salisbury J K, Craig J J. Articulated hands: force control and kinematic issues. *The International Journal of Robotics Research*, 1982, 1(1): 4–17
3. Jacobsen S C, Wood J E, Knutti D F, Biggers K B. The UTAH/M.I.T. dextrous hand: work in progress. *The International Journal of Robotics Research*, 1984, 3(4): 21–50
4. Bridgwater L B, Ihrke C A, Diftler M A, Abdallah M E, Radford N A, Rogers J M, Yayathi S, Askew R S, Linn D M. The Robonaut 2 hand—designed to do work with tools. In: Proceedings of 2012 IEEE International Conference on Robotics and Automation. Saint Paul: IEEE, 2012, 3425–3430
5. Butterfass J, Grebenstein M, Liu H, Hirzinger G. DLR-hand II: next generation of a dextrous robot hand. In: Proceedings of 2001 ICRA. IEEE International Conference on Robotics and Automation. Seoul: IEEE, 2001, 109–114
6. Liu H, Wu K, Meusel P, Seitz N, Hirzinger G, Jin M H, Liu Y W, Fan S W, Lan T, Chen Z P. Multisensory five-finger dexterous hand: the DLR/HIT hand II. In: Proceedings of 2008 IEEE/RSJ International Conference on Intelligent Robots and Systems. Nice: IEEE, 2008, 3692–3697
7. Hurst J W, Chestnutt J E, Rizzi A A. An actuator with physically variable stiffness for highly dynamic legged locomotion. In: Proceedings of IEEE International Conference on Robotics and Automation. New Orleans: IEEE, 2004, 5: 4662–4667
8. Wolf S, Hirzinger G. A new variable stiffness design: matching requirements of the next robot generation. In: Proceedings of 2008 IEEE International Conference on Robotics and Automation. Pasadena: IEEE, 2008, 1741–1746
9. Lotti F, Tiezzi P, Vassura G, Biagiotti L, Palli G, Melchiorri C. Development of UB hand 3: early results. In: Proceedings of the 2005 IEEE International Conference on Robotics and Automation. Barcelona: IEEE, 2005, 4488–4493
10. Teeple C B, Koutros T N, Graule M A, Wood R J. Multi-segment soft robotic fingers enable robust precision grasping. *The International Journal of Robotics Research*, 2020, 39(14): 1647–1667
11. Wolf S, Eiberger O, Hirzinger G. The DLR FSJ: energy based design of a variable stiffness joint. In: Proceedings of 2011 IEEE International Conference on Robotics and Automation. Shanghai: IEEE, 2011, 5082–5089
12. Tsagarakis N G, Sardellitti I, Caldwell D G. A new variable stiffness actuator (CompAct-VSA): design and modelling. In: Proceedings of 2011 IEEE/RSJ International Conference on Intelligent Robots and Systems. San Francisco: IEEE, 2011, 378–383
13. Choi J, Hong S, Lee W, Kang S. A variable stiffness joint using leaf springs for robot manipulators. In: Proceedings of 2009 IEEE International Conference on Robotics and Automation. Kobe: IEEE, 2009, 4363–4368
14. Catalano M G, Grioli G, Bonomo F, Schiavi R, Bicchi A. VSA-HD: from the enumeration analysis to the prototypical implementation. In: Proceedings of 2010 IEEE/RSJ 2010 International Conference on Intelligent Robots and Systems. Taipei: IEEE, 2010, 3676–3681
15. Grebenstein M, Chalon M, Hirzinger G, Siegwart R. Antagonistically driven finger design for the anthropomorphic DLR hand arm system. In: Proceedings of 2010 the 10th IEEE-RAS International Conference on Humanoid Robots. Nashville: IEEE, 2010, 609–616
16. Koyama K, Shimojo M, Senoo T, Ishikawa M. Development and application of low-friction, compact size actuator “MagLinkage”. *The Proceedings of JSME annual Conference on Robotics and Mechatronics (Robomec)*, 2019, 2P1–H02
17. Walkler R. Developments in dextrous hands for advanced robotic applications. In: Proceedings of World Automation Congress. Seville: IEEE, 2004, 123–128
18. Moura T, Kawasaki H, Yoshikawa K, Takai J, Ito S. Anthropomorphic robot hand: Gifu Hand III. In: Proceedings of International Conference on Control, Automation, and Systems. Jeonbuk, 2002, 1288–1293
19. Ficuciello F, Palli G, Melchiorri C, Siciliano B. Experimental evaluation of postural synergies during reach to grasp with the UB hand IV. In: Proceedings of 2011 IEEE/RSJ International Conference on Intelligent Robots and Systems. San Francisco: IEEE, 2011, 1775–1780
20. Chalon M, Wedler A, Baumann A, Bertleff W, Beyer A, Butterfaß J, Grebenstein M, Gruber R, Hacker F, Kraemer E, Landzettel K, Maier M, Sedlmayr H J, Seitz N, Wappler F, Willberg B, Wimboeck T, Hirzinger G, Didot F. Dexhand: a space qualified multi-fingered robotic hand. In: Proceedings of 2011 IEEE International Conference on Robotics and Automation. Shanghai: IEEE, 2011, 2204–2210
21. Grebenstein M. The Awiwi Hand: an Artificial Hand for the DLR Hand Arm System. Cham: Springer, 2014
22. Quigley M, Salisbury C, Ng A Y, Salisbury J K. Mechatronic design of an integrated robotic hand. *The International Journal of Robotics Research*, 2014, 33(5): 706–720

23. Ruehl S W, Parlitz C, Heppner G, Hermann A, Roennau A, Dillmann R. Experimental evaluation of the schunk 5-finger gripping hand for grasping tasks. In: Proceedings of 2014 IEEE International Conference on Robotics and Biomimetics (ROBIO 2014). Bali: IEEE, 2014, 2465–2470
24. Grossard M, Martin J, da Cruz Pacheco G F. Control-oriented design and robust decentralized control of the CEA dexterous robot hand. *IEEE/ASME Transactions on Mechatronics*, 2015, 20(4): 1809–1821
25. Fang B, Sun F C, Chen Y, Zhu C, Xia Z W, Yang Y Y. A tendon-driven dexterous hand design with tactile sensor array for grasping and manipulation. In: Proceedings of 2019 IEEE International Conference on Robotics and Biomimetics (ROBIO). Dali: IEEE, 2019, 203–210
26. Kim Y J, Yoon J, Sim Y W. Fluid lubricated dexterous finger mechanism for human-like impact absorbing capability. *IEEE Robotics and Automation Letters*, 2019, 4(4): 3971–3978
27. Vanderborght B, Albu-Schaeffer A, Bicchi A, Burdet E, Caldwell D G, Carloni R, Catalano M, Eiberger O, Friedl W, Ganesh G, Garabini M, Grebenstein M, Grioli G, Haddadin S, Höppner H, Jafari A, Laffranchi M, Lefèber D, Petit F, Stramigioli S, Tsagarakis N, Van Damme M, Van Ham R, Visser L C, Wolf S. Variable impedance actuators: a review. *Robotics and Autonomous Systems*, 2013, 61(12): 1601–1614
28. Wolf S, Grioli G, Eiberger O, Friedl W, Grebenstein M, Höppner H, Burdet E, Caldwell D G, Carloni R, Catalano M G, Lefèber D, Stramigioli S, Tsagarakis N, Van Damme M, Van Ham R, Vanderborght B, Visser L C, Bicchi A, Albu-Schäffer A. Variable stiffness actuators: review on design and components. *IEEE/ASME Transactions on Mechatronics*, 2016, 21(5): 2418–2430
29. Catalano M G, Grioli G, Garabini M, Bonomo F, Mancini M, Tsagarakis N, Bicchi A. VSA-cubebot: a modular variable stiffness platform for multiple degrees of freedom robots. In: Proceedings of 2011 IEEE International Conference on Robotics and Automation. Shanghai: IEEE, 2011, 5090–5095
30. Jafari A, Tsagarakis N G, Sardellitti I, Caldwell D G. A new actuator with adjustable stiffness based on a variable ratio lever mechanism. *IEEE/ASME Transactions on Mechatronics*, 2014, 19(1): 55–63
31. Shao Y X, Zhang W X, Ding X L. Configuration synthesis of variable stiffness mechanisms based on guide-bar mechanisms with length-adjustable links. *Mechanism and Machine Theory*, 2021, 156: 104153
32. Oh J, Lee S, Lim M, Choi J. A mechanically adjustable stiffness actuator (MASA) of a robot for knee rehabilitation. In: Proceedings of 2014 IEEE International Conference on Robotics and Automation (ICRA). Hong Kong: IEEE, 2014, 3384–3389
33. Shao Y X, Zhang W X, Su Y J, Ding X L. Design and optimisation of load-adaptive actuator with variable stiffness for compact ankle exoskeleton. *Mechanism and Machine Theory*, 2021, 161: 104323
34. Grebenstein M, van der Smagt P. Antagonism for a highly anthropomorphic hand-arm system. *Advanced Robotics*, 2008, 22(1): 39–55
35. Petit F, Friedl W, Höppner H, Grebenstein M. Analysis and synthesis of the bidirectional antagonistic variable stiffness mechanism. *IEEE/ASME Transactions on Mechatronics*, 2015, 20(2): 684–695
36. Grebenstein M, Chalon M, Friedl W, Haddadin S, Wimböck T, Hirzinger G, Siegwart R. The hand of the DLR hand arm system: designed for interaction. *The International Journal of Robotics Research*, 2012, 31(13): 1531–1555